PERGAMON

Acta mater. 48 (2000) 635–646

Acta MATERIALIA

www.elsevier.com/locate/actamat

LATENT STRAIN IN TITANIUM–NICKEL THIN FILMS MODIFIED BY IRRADIATION OF THE PLASTICALLY-DEFORMED MARTENSITE PHASE WITH 5 MeV Ni^{2+}

DAVID S. GRUMMON[1]† **and ROLF GOTTHARDT**[2]

[1]Department of Materials Science and Mechanics, Michigan State University, East Lansing, MI 48824-1226, USA and [2]Institute de Génie Atomique, Departement du Physique, École Polytechnique Fédérale de Lausanne, Switzerland

(Received 29 June 1999; received in revised form 27 October 1999; accepted 27 October 1999)

Abstract—Lattice damage brought on by heavy ion irradiation is able to alter the displacive transformation characteristics of near equiatomic titanium–nickel. Irradiation of sputtered TiNi thin films can modify thermomechanical response to a depth of more than a micron, and may thus be used to create a perfectly bonded heterophase that deploys materials of sharply differing latent thermal strain on opposite sides of a thin sheet. If the alloy film is first martensitized, and then deformed in tension prior to partial-depth exposure to ion beam damage at temperatures well below A_s, a novel active-passive bilayer results that expresses pronounced bending displacements on subsequent heating. In the present paper, describing experiments on stretched 6-μm thick sputtered $Ti_{50.2}Ni_{49.7}$ films irradiated with 5 MeV Ni^{2+}, we show that ion-induced latent bending can be cyclically reversed in temperature-displacement space, and that appreciable mechanical work can be extracted. Marked effects are observed at doses as low as 5×10^{13} Ni^{2+} cm^{-2}. The approach, in which nominally planar processing is used, derives mechanical robustness from a naturally diffuse interface between the beam-damaged stratum and the adjacent unmodified shape-memory layer.

Keywords: Ion beam methods (implantation); Martensite/shear; Multilayers; Thermomechanical shape memory; Thin films

1. INTRODUCTION

Because of their anomalously high strain energy output (exceeding 10 MJ/m^3 [1]), thin films of equiatomic titanium–nickel are of considerable current interest as an enabling material for actuators at the sub-millimeter scale. The general robustness of the shape-memory effect in sputtered titanium–nickel films has been amply demonstrated [2–8]. Shape-memory arises when large plastic strains, mediated by twin- and variant-boundary motion in the low temperature, low-symmetry martensite phase, are subsequently recovered during the first-order endothermal transformation to a high-symmetry austenite phase on heating. To obtain a useful force·displacement product from the effect it is thus necessary to provide for plastic deformation of the martensite phase, usually by means of a coupled elastic 'biasing' element. In macroscopic applications, provision of biasing (resetting) forces to induce strains beyond 5% poses little difficulty, but in the spatially and dimensionally constrained setting of microelectro-mechanical systems (MEMS), attachment of biasing elements and deformation of the martensite become more awkward, and a nominally planar approach to biasing, compatible with thin-film lithographic techniques, is desirable. In principle, if a martensitic thin film has been initially deformed, planar biasing can be effected by provision of an intimately bonded parallel elastic layer which enforces an out-of-plane bending displacement during the martensite → austenite transformation on heating, and then re-deforms the martensite on cooling. Cyclic actuation at a scale appropriate to MEMS technologies can thus be achieved by the conversion of a fractional layer of the deformed martensite into a strong but conventionally elastic stratum, which is able to store elastic strain energy during shape-changes (on heating), and make them available to reset the martensite phase on subsequent cooling.

In the present work, a planar elastic zone has

† To whom all correspondence should be addressed.

1359-6454/00/$20.00
PII: S1359-6454(99)00401-2

been produced *in situ* by heavy ion irradiation of one side of a deformed martensitic (B19′) TiNi thin film.† The aim of the experiment was to produce sufficient lattice damage to frustrate the reverse-transformation to the austenite (B2) phase, in a 1–2-μm-thick layer on one side of the film, leading to pronounced out-of-plane bending strain on heating past the A_f temperature. This sort of displacement could in principle be harnessed to perform useful work in microelectromechanical systems. To the extent that the irradiated zone responds in a nominally elastic fashion during reversion, a significant amount of elastic strain energy is stored in the elastic layer and becomes available to redeform the film on cooling, leading to the realization of an extrinsically biased two-way cyclic actuator element.

A similar effect could be produced with simple deposition of a discrete elastic layer, by more conventional means, but the use of ion irradiation provides the final heterostructure with a broadly diffuse interface between the thermotractive and conventionally-elastic zones. This minimizes interfacial shear stress concentration and reduces the tendency toward delamination which would otherwise be expected at the high stresses and strains encountered during thermal cycling.

Little is presently known about the response of the martensite phase in TiNi to heavy-ion irradiation. In neutron irradiation studies on austenitic materials by Hoshiya *et al.* [9, 10] it was found that the M_s temperature could be lowered by 80–200 K using fast neutron irradiation to doses of $\sim 10^{-2}$ displacements per atom (DPA) at 323 K, but that dynamic ordering occurred at temperatures above 520 K, resulting in little change in transformation characteristics. Similarly, TiPd alloys were found to disorder under neutron irradiation at doses below 0.01 DPA for irradiation below 333 K (at which temperature the martensite phase should have been stable), but remained ordered to doses greater than 0.1 DPA for irradiation above 500 K [11]. Complete amorphization of TiNi can be achieved by proton irradiation at 0.32 DPA (at 228 K) and 0.25 DPA (at 120 K) [12], with partially amorphous structures containing still-ordered B2 phase occurring at 0.15 DPA. He^+ irradiations on 2.5-μm-thick ion-sputtered austenitic TiNi films, to damage levels as high as 0.007 DPA, lowered M_s and A_s by 5 and 7 K, respectively, and suppressed the R-phase transformation at doses greater than 0.003 DPA [13]. Brimhall *et al.* [14] investigated Ni^+ and Ta^{3+} irradiation at 2.5 and 6.0 MeV, respectively, and found complete amorphization in both cases to occur at doses above ~0.1 DPA at nominally ambient temperature. Significantly in these experiments, the long range order parameter was found to fall to 0.6 at doses as low as 0.05 DPA for 2.5 MeV Ni^+ irradiation.

In general, studies to date have indicated that the transformation temperatures, M_s, M_f, A_s and A_f are lowered in response to beam damage, implying that sub-amorphization doses could decrease A_s enough, depending on the heat sink temperature, to trigger *in situ* reversion of the martensite during irradiation. One aim of the present work has therefore been to investigate the shape-recovery which may result directly from such radiation-induced austenite formation in a pre-deformed martensite, especially when the heat-sink temperature is not too far below A_s. Further, since shape-memory depends critically on not only the lattice symmetries, but also the lattice ordering (which enforces a single crystallographic reversion path for the $M \rightarrow A$ transformation) it is also of interest to determine whether ion doses significantly below the amorphization fluence can fully frustrate strain recovery from shape-memory effects. If so, it is useful to determine if a useful level of elastic strain energy can be stored in the beam-damaged layer, or whether excessive plastic deformation (or fracture) would occur in response to a thermotractive shape recovery in the undamaged layer.

In this preliminary experiment we have attempted to establish the irradiation fluence required to inhibit reverse-transformation in a deformed TiNi martensite, and to observe the mechanical response of the films both to irradiation alone, and to post-irradiation thermal cycling, in materials bombarded at different temperatures.

2. EXPERIMENTAL PROCEDURES

2.1. Technical approach

The general approach to the experiment is illustrated in Fig. 1. In step (1) a binary TiNi thin film designed to have an M_f temperature above 320 K and an A_s temperature above ~350 K is fabricated by magnetron sputtering and post-deposition annealing. In step (2) the martensitic film, after release from its substrate, is deformed in uniaxial tension to a plastic strain of between 3 and 5%, and thereafter kept cool enough to prohibit reversion to the austenite. In step (3) the deformed film is mounted on an efficient heat-sinking fixture and irradiated at high energy with heavy ion species while the specimen temperature is kept rigorously below A_s. In step (4) the irradiated film is removed from the heat sink and mounted on a fixture which allows convenient measurement of out-of-plane

† Although plastic deformation was effected manually on a free-standing film in these experiments, in principle such deformation can be accomplished *in situ*, for elements on (100)Si, by accumulating differential thermal expansion strains during cooling from a stress-free state at high temperature. These can be subsequently annihilated by displacive transformation at near room temperature [15] to provide the initial martensite strain.

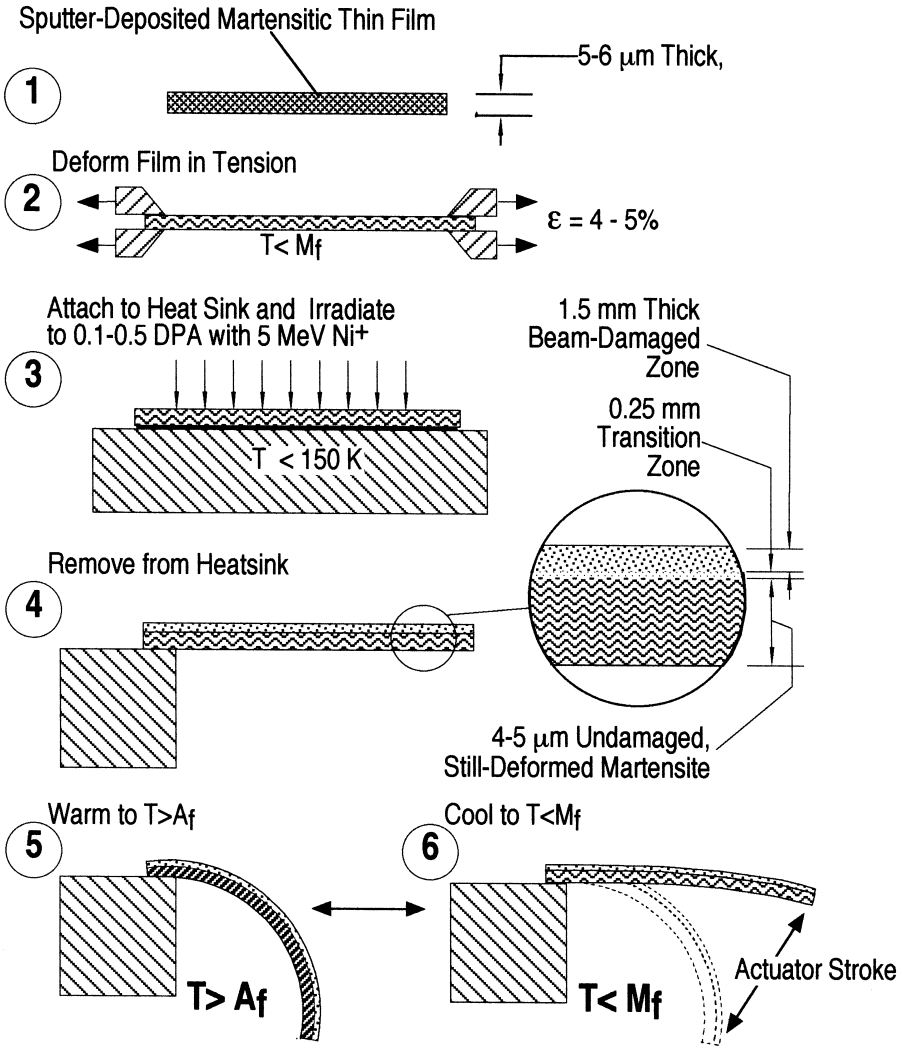

Fig. 1. Schematic sequence for the generation of reversible out-of-plane displacement by irradiating a deformed TiNi thin film martensite.

bending displacement during step (5), in which the film is finally heated above the A_f temperature. In step (6), the specimen is again cooled below M_f to determine the degree to which stored elastic strain energy in the damaged layer is capable of re-deforming the martensite phase. Finally, steps (5) and (6) are repeated for several cycles to determine the post-shakedown amplitude of the cyclic displacement capability.

Step (3) was carried out with the aid of the transport calculations† given in Fig. 2, which indicate that at 5 MeV a dose of 10^{14} cm^{-2} will produce vacancy-forming displacements to a peak level of ~0.3 vacancies per atom at a depth of 1.2–1.5 μm, and an average implanted nickel concentration of ~45 ppm. The calculated average damage level for a fluence of 10^{14} cm^{-2} was 0.19 DPA.

2.2. Procedures

Several thin films, each approx. 6 μm thick, were fabricated by diode magnetron sputter deposition at 2.5 mTorr argon pressure, at a substrate temperature of 280°C, cathode power 200 W, from $Ti_{50.2}Ni_{49.8}$ alloy targets augmented with four 3.1-mm diameter pure-Ti rods inserted in the wear track. The as-sputtered films were amorphous and slightly Ti-rich. The films were peeled from their silicon substrates and then vacuum annealed between quartz plates at 300°C for 1 h and at 550°C for 2 h, followed by furnace cooling. The as-

† TRIM:SRIM-98 (98.01); 500 atoms of $^{28}Ni^{2+}$ into $Ti_{50}Ni_{50}$ with density = 7.288 atoms/cm^3; total ions calculated = 500; displacement energy = 25 eV for Ni and Ti, lattice binding energy = 2 eV. The units of Nv and Ni per Å-ion on the lefthand scales in Fig. 2 are understood as (N/Å^3)/(ions/Å^2).

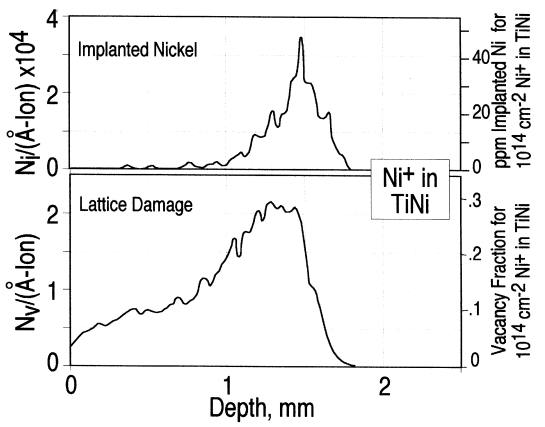

Fig. 2. Results of transport calculations showing the projected ion range and the damage production level as a function of depth for 5 MeV Ni^+ in equiatomic TiNi.

annealed films were fully martensitic at room temperature and displayed M_f and A_s temperatures of approx. 40 and 75°C respectively, as indicated by the differential calorimetry scan shown in Fig. 3, which applies to all of the specimens used in the present study. As is the general case for films given a post-deposition crystallization anneal, the films had a grain size of approx. 1 μm and were not textured.

Individual strips were mechanically cut by hand to lengths between 45 and 60 mm and widths of 4–6 mm. Stainless steel washers were glued to the ends of these strips with epoxy adhesive to function as pin-loaded grips. The strips were then mounted on a micrometer-driven stage and manually stretched in tension to produce plastic strains between 2.6 and 4.8%. Most of the films were strained to fracture in this manner. After deformation, a 1-mm wide strip was cut parallel to the tensile axis of each of the deformed strips, placed loosely between two microscope slides, and measured on a Mitutoyo PJ311 Profile Projector to

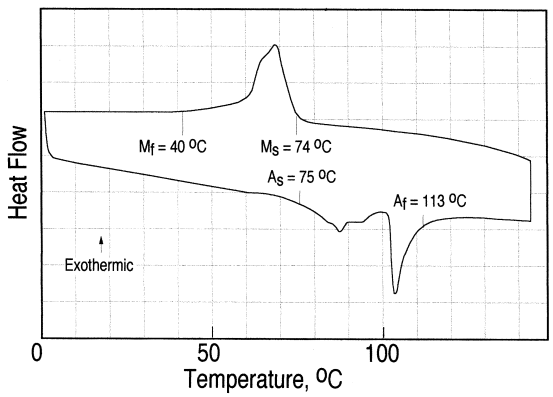

Fig. 3. Differential Scanning calorimetry scan of the as-deposited specimen material used in the study.

a resolution of 1 μm. The 1-mm strips were then heated past the A_f temperature and measured again (at room temperature) to determine the recovered shape-memory strain. The remaining deformed material was cut into 12–15-mm lengths, each 4–5 mm wide, and stored at room temperature prior to irradiation.

Specimen F301 was mounted on to a LN_2-cooled copper cryostat and irradiated at 133 K for 45 min with 5.0 MeV Ni^{2+} ions at beam currents between 100 and 175 nA, covering an area of 0.6 cm^2. The total resulting ion charge of 1.92×10^{-4} coulombs corresponds to a dose (corrected for the double charge) of 1×10^{15} Ni^{2+} cm^{-2}.

Specimens F801, F802 and F803 were mounted to a 4-mm-thick plate copper heat sink using graphite paint then irradiated at ambient temperature in the same facility at a beam current of 50 nA for 32 min, 6 min 40 s, and 3 min 20 s, resulting in doses of 5×10^{14}, 1×10^{14} and 5×10^{13} cm^{-2} respectively. For all of the irradiations, the target chamber pressure was below 4×10^{-6} Torr. Table 1 summarizes the martensite deformation and irradiation conditions for the four thin films and gives the calculated lattice damage level. (The actual temperature rise in the irradiation zone for F801, F802 and F803 could not be accurately determined for the specimens processed at ambient chamber temperature).

After irradiation, the end of each specimen was gripped between a pair of glass microscope slides in a cantilevered position and indirectly heated in still air while the free displacement was recorded at low magnification using a video camera and microscope.

A very approximate experimental measurement of the force output of one of the irradiated thin film elements was made by observing the deflection of a micromachined stainless steel cantilever beam which was positioned in contact with the free end of the film element. The 10-mm-long calibrated beam, with a 100×100 μm square cross-section, had a force–displacement characteristic of 16 N/m of tip deflection. The specimen was mounted in a grip made from glass plates such that one end of the film was fixed, and the remaining curved portion (including the entire irradiated area) was cantilevered with the free end positioned to contact the steel beam, as shown in Fig. 4. A small resistance heater positioned below the film was used to excite the martensite to austenite transformation, and the resulting beam deflection was monitored with a computerized optical tracking system.

A limited number of nanoindentation hardness measurements were made on the irradiated side of specimens F301, F803, and on an unirradiated control film. The films were bonded tightly to glass substrates with cyanoacrylate adhesive after the completion of the temperature-displacement observations (i.e. after several thermal cycles between

Table 1

Thin film specimen	Strain recovery experiment			Irradiated specimen dimensions	Irradiation conditions				
	L_0 (mm)	L_f	Strain		Temp (K)	Time (m:s)	Current (nA)	Total dose (cm^{-2})	Damage (DPA)
F301	27.91	26.682	4.42%	4.5×12.1	−133 K	25:00	100–175	1×10^{15}	1.90
F801	32.11	30.619	4.66%	4.9×14.5	> 300 K	32:00	50	5×10^{14}	0.95
F802	36.84	35.283	4.24%	4.9×13.1	> 300 K	6:40	50	1×10^{14}	0.19
F803	27.91	26.682	4.42%	4.2×15.4	> 300 K	3:20	50	5×10^{13}	0.095

ambient temperature and ~70–120°C). A NanoIndenter-II instrument fitted with a standard Berkovitch indenter was used, and measurements were made at room temperature.

3. RESULTS

3.1. Initial response to irradiation

Irradiation at all doses studied produced no obvious discoloration or surface texturing to the thin film specimens, but the extent of the irradiation zone could be discerned by a very slight discoloration of the graphite paint surrounding the films. This zone was in all cases approx. 6.4 mm long (in the direction of the specimen tensile axis) and covered the full width of each specimen. After irradiation, specimens for all the irradiations remained attached to their heat sinks and no gross curvature was observed. However, at the edges of the irradiation zone for specimen F301, irradiated at 133 K, a small amount of macroscopic surface relief was apparent, indicating a slight concavity toward the irradiated face, parallel to the edge of each irradiation-zone, approximately as shown in a slightly exaggerated schematic view in Fig. 5(a). Specimen F803 (5×10^{13} cm^{-2} dose), when released from the heat sink by dissolving the carbon paint adhesive in acetone, spontaneously curled toward the irradiated side, which brought the free end of the strip into self-contact, as shown in Fig. 5(b). Specimen F802 (1×10^{14} cm^{-2} dose) also curved toward the irradiated side when released from the heat sink, but not sufficiently to produce self-contact. Specimen F801 showed less curvature than -802 or -803, and F301 did not show any tendency toward such curvature when released from the heat sink.

3.2. Thermal cycling response

Profiles indicating the curvature adopted during the first heating excursion above A_f, and during subsequent thermal cycling of the irradiated films, are shown in Figs 6–9, together with time-temperature curves for each experiment. The profiles shown give qualitative schematic views of the appearance of the films viewed edge-on, as sketched from the video recording made during thermal cycling. In general, the first profile shows the post-irradiation curvature, which was concave toward the irradiated face for all but the highest dose irradiation (F301). As temperature was increased, all specimens responded with the evolution of complex shapes associated with the development of curvature radii of different sign, depending on the temperature and

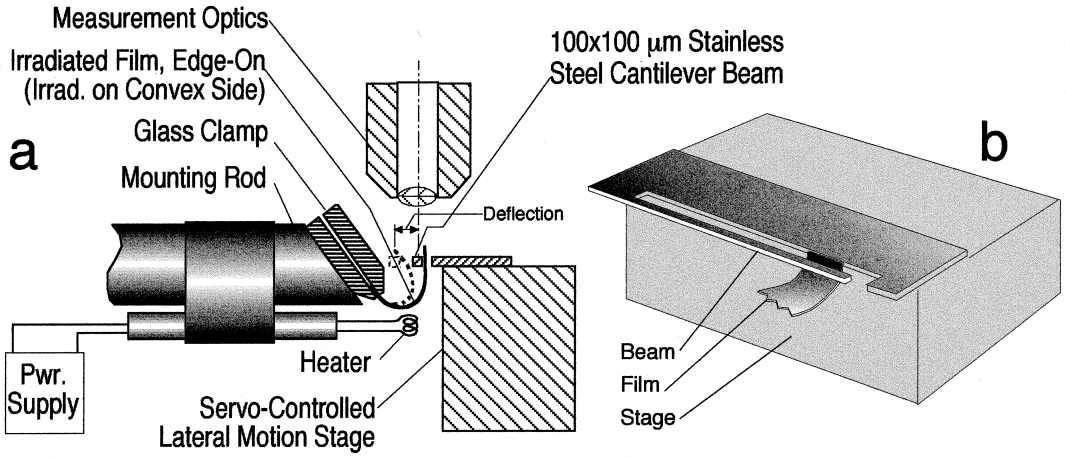

Fig. 4. Schematic sketches of the apparatus used to make force output measurements during heating of an irradiated specimen. The glass clamp used to hold the specimen was glued to the end of a 9.5-mm-diameter aluminum rod.

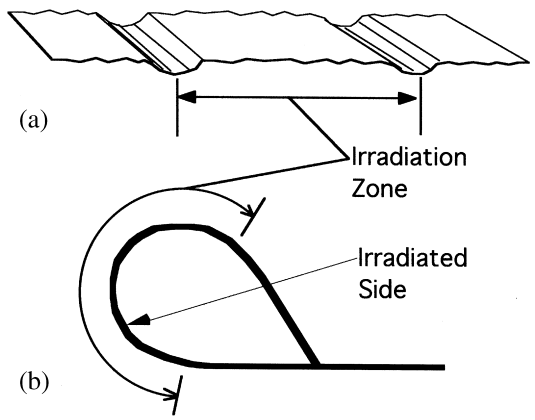

Fig. 5. (a) Slight curvature noted at the ends of the irradiation zone in some irradiated specimens. (b) Concave curvature noted in some specimens after release from the irradiation fixture.

location along the specimen's long axis with respect to the extent of the irradiation zone. Increased curvature, concave toward the irradiated face (right side in Figs 6–9), was frequently observed early in the first heating excursion, and was often more pronounced at one or both edges of the irradiation zone.

In all cases, however, irradiated specimens eventually developed a pronounced convex curvature (concave *away* from the irradiated face, i.e. concave to the left in Figs 6–9) as the A_s temperature of the undamaged material (70–75°C) was approached. This curvature was substantially reversed (but not always completely) on cooling below the M_f temperature. For each data set shown in Figs 6–9, the last two profiles on the right are the approximate 'closed' (warm) and 'open' (cool) configurations of the films, and subsequent thermal cycling between M_f and A_s caused the shape to alternate between these extremes for at least 10 cycles. It should be noted that in many cases, the maximum free displacement (curvature to smaller radii) was frustrated by contact of the free end of the film with itself, or with parts of the fixturing. All bending was confined to the axial sense, and no warping or twisting was observed. In some cases, however, it was apparent that slight transverse curvatures (mostly introduced as artifacts of handling) inhibited bending strain in one direction until mild pop-through buckling events occurred. Unirradiated specimens, deformed in the martensitic state using the same procedures as for irradiated materials, remained flat and showed no out-of-plane deformation when heated past the A_f temperature.

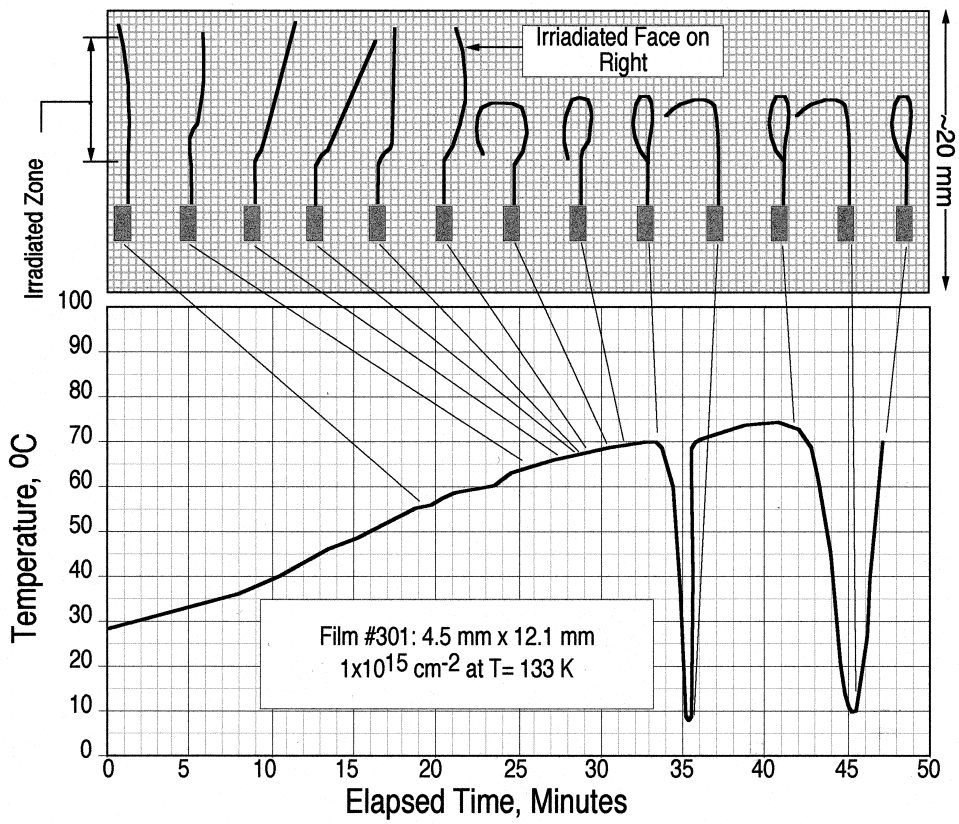

Fig. 6. Schematic displacement as a function of time and temperature for irradiated specimen F301.

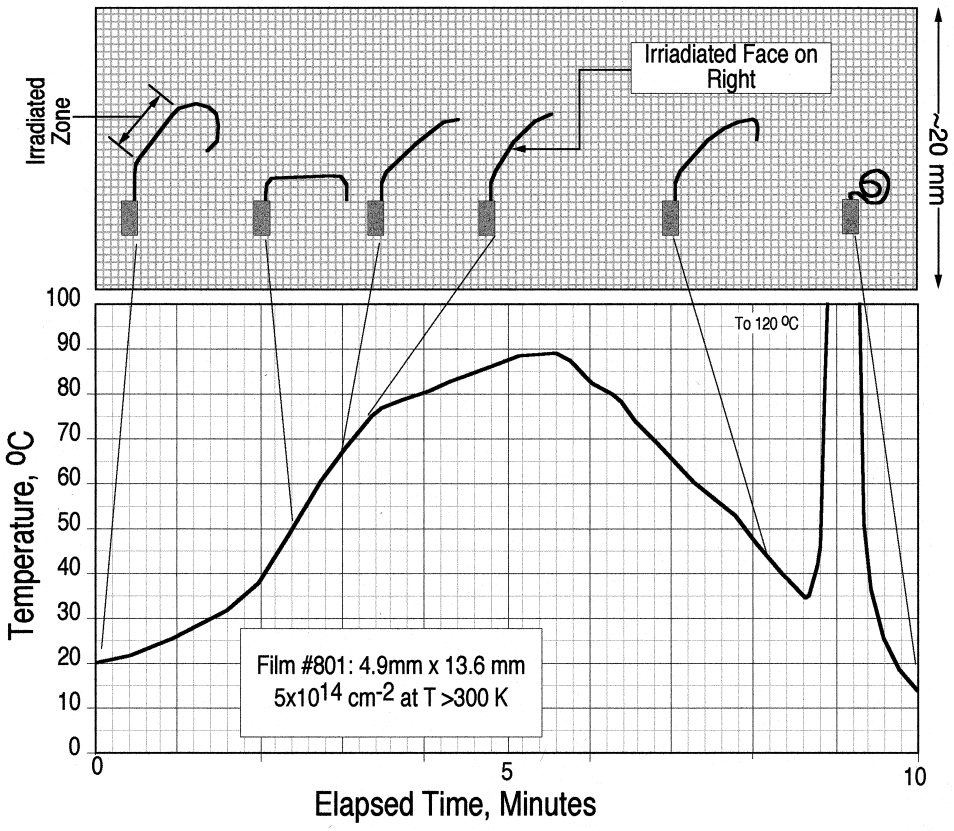

Fig. 7. Schematic displacement as a function of time and temperature for irradiated specimen F801.

3.3. Force measurements

After several cycles of thermal excursion between 20 and 70°C, specimen F301 (1×10^{15} cm^{-2} dose) was curved away from the irradiated face to a radius of approx. 3 mm at room temperature, and when heated would curve more tightly (as shown in the last two frames at the top of Fig. 6) until self-contact constrained further bending displacement. In order to estimate the force output developed when this bending strain was constrained during heating, specimen F301 was mounted in an apparatus such that the force developed produced a strain in a calibrated stainless steel microcantilever. The measured force output is shown as a function of time for two heating excursions in Fig. 10. The flattened peaks in the force output curves correspond to the displacement limit of the optical tracking system used, indicating that the maximum output was beyond the measurement range of the force-transducer, which registered a maximum of approx. 11.4 mN at a beam displacement of 720 μm. However, direct microscopic observation of the bending beam, scaled to the known dimensions of the measurement unit, indicated a maximum constrained displacement of end of the beam of approx. 1.5 mm, corresponding to a force output of 0.024 N at the maximum temperature. Approximately the same displacement was achieved in two separate thermal cycles. (The temperature at maximum displacement could not be accurately measured in this apparatus, but is estimated to be ~120°C).

3.4. Nanoindentation hardness

Specimens F301, F802 and an unirradiated control film were subjected to nanoindentation hardness measurements using a Berkovitch indenter. For each specimen, three to four indents were made, at 1000 nm indentation depths, at points spaced 25 μm apart. Figure 11 shows three load–displacement curves for specimen F301 (1×10^{15} cm^{-2} dose). (Curves obtained for the low-dose implanted specimen and the unirradiated control film were qualitatively similar and are not shown.) Hardness and elastic modulus data derived from these measurements are shown in Figs 12(a) and (b) for the three specimens. The high-dose specimen shows a sharp increase in superficial hardness, from a maximum of 2.75 GPa for the control, to over 8 GPa for the specimen irradiated to a dose of 1×10^{15} cm^{-2}. For the specimen irradiated with 5×10^{13} cm^{-2} Ni^{2+}, the increase in hardness is much more modest, but still discernable at indent depths less than 550 nm. A similar trend is evident in the elastic modulus

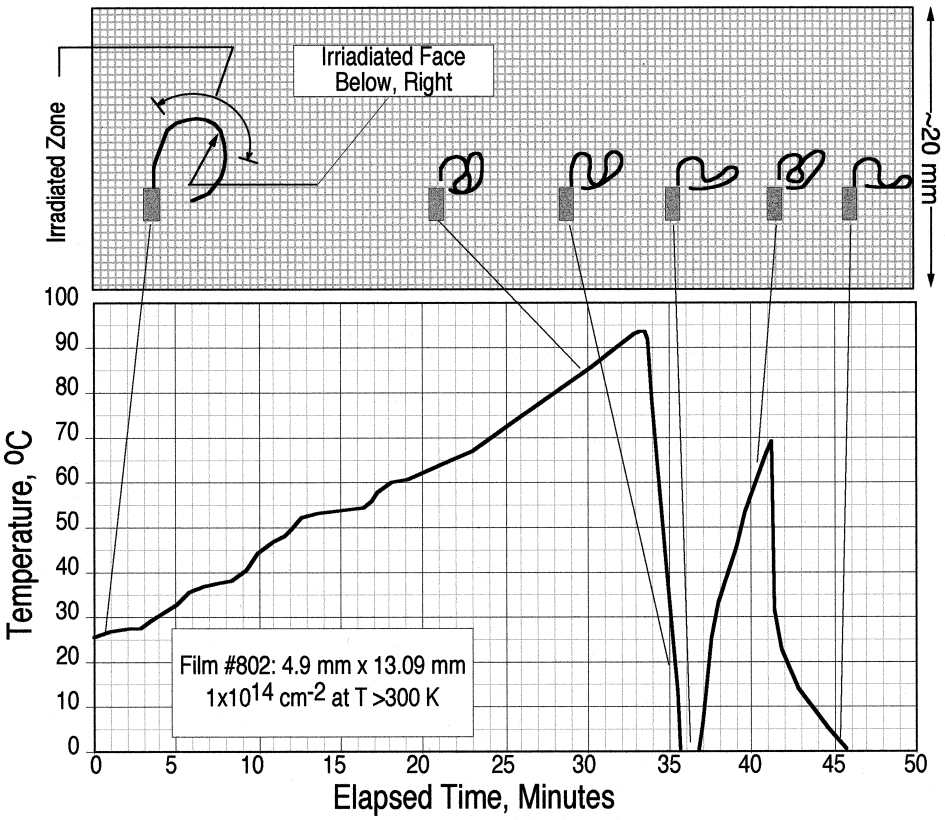

Fig. 8. Schematic displacement as a function of time and temperature for irradiated specimen F802.

data in Fig. 12(b). Here, the highest dose is shown to produce a sharp rise in the apparent modulus compared to the control and low-dose irradiation. Though data at greater depths are not available, the curve for specimen F310 appears to converge with the control curve at a depth of 1.8 μm, close to the end of the ion range shown in Fig. 2. The modulus at a depth of 1 μm for the control specimen (20 GPa) is typical for TiNi martensites. The high peak values (> 100 GPa) for specimen 301 are indicative of irradiation induced austenitization or amorphization, but may not accurately reflect the actual properties of the irradiated zone since the depth of the modified surface layer is on the order of the indent depth. However, it is clear that irradiation at 5×10^{15} cm^{-2} substantially alters the strength and stiffness of an initially martensitic TiNi thin film, and that irradiation of the martensite to a fluence of 5×10^{13} cm^{-2} Ni^{2+} at 5 MeV is close to the threshold for significant alteration of these properties.

4. DISCUSSION

The pre-deformed and irradiated titanium–nickel martensites in this study exhibited complex bending behavior both in direct response to irradiation, and in response to post-irradiation thermal cycling between $T < M_f$ and $T > A_f$. Bending curvatures of differing sign occurred at different temperatures, and at different locations along the specimen axis in relationship to the irradiated zone. The immediate response to irradiation also appeared to depend on the irradiation temperature. For irradiation to high fluence at very low temperature (133 K), no gross curvature resulted directly from beam exposure, except for a very slight effect at the margins of the irradiated zone. For irradiation at ambient temperature (and to lower doses), a substantial, general curvature occurred upon release from the fixturing, which was in all cases concave toward the irradiated face, and tended to be somewhat more exaggerated at the margins of the irradiated zone.

For all except specimen F301, interpretation of the direct effect of irradiation is complicated by uncertainty regarding the actual specimen temperature during irradiation in relation to A_s. Heat removal from the specimen was accomplished principally by conduction through the thermal mass of the copper heat sink, and with 50 nA beam current and 5 MeV energy, the 250 mW thermal load would have slowly warmed this 450 g mass by about 3.5 K over the 41 min total irradiation interval. However, because bonding to the heat sink was imperfect, and because the thermal conductivity of TiNi is poor, local surface heating from this power

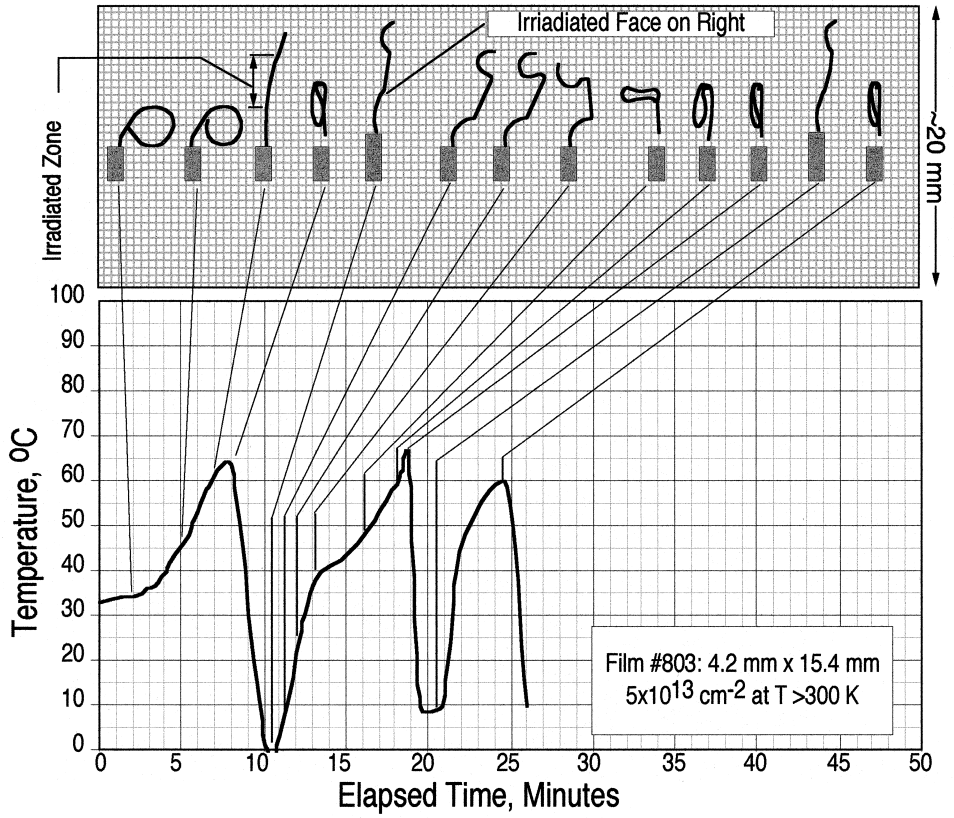

Fig. 9. Schematic displacement as a function of time and temperature for irradiated specimen F803.

input may have been appreciable within the beam-damage zone. Since the nominal heat sink temperature was within 50–60 K of the A_s temperature, it cannot be ruled out that some beam-induced austenitization occurred *in situ* for specimens F801, F802 and F803. Since the parent martensite in this case had been deformed, such beam-heating-induced reversion may account for some of the observed bending curvature toward the irradiated side after release from the fixture. Furthermore, since it may be presumed, based on the few available published results and the general tendency for lattice imperfection to lower the canonical transformation temperatures in shape-memory materials, that irradiation which did not induce amorphization would lower the A_s temperature, perhaps enough to initiate austenitization in combination with concurrent beam-heating. It is an open question, however, as to the strains that would be expected under these circumstances. For example, if the cascade model of beam–solid interaction is considered, it is not clear what shape-strain would result even if the phase

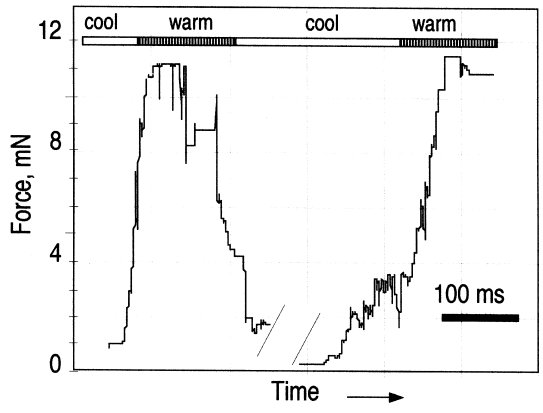

Fig. 10. Force output as a function of time for two heat/cool cycles applied to specimen F301 using the apparatus shown in Fig. 4.

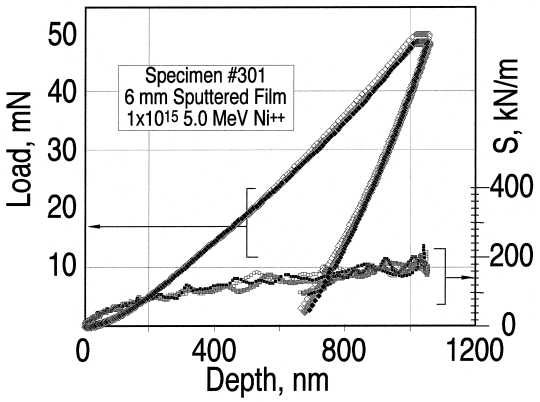

Fig. 11. Nanoindentation response of specimen F301.

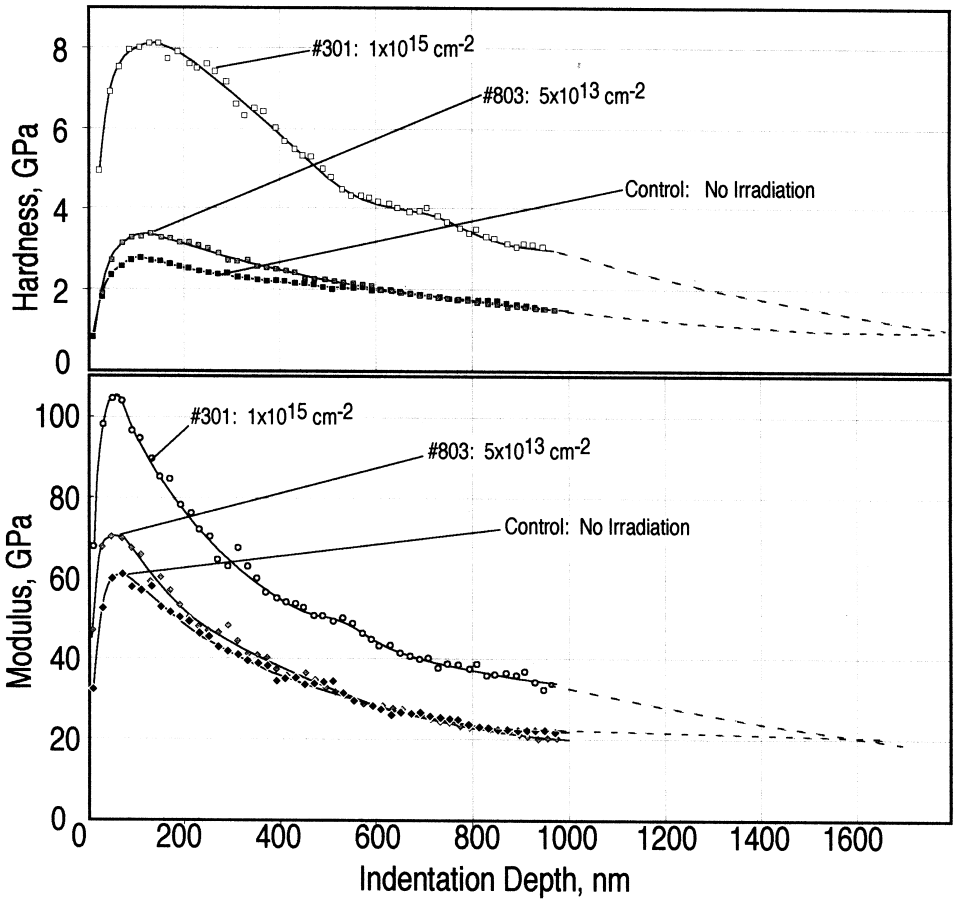

Fig. 12. Modulus and hardness as a function of depth below the surface for films irradiated at various doses.

which predominated after the annealing of a displacement spike were a crystalline austenite descended from a pre-deformed martensite. These austenites would not necessarily confer much shape-strain if they were nucleated with crystallographic orientations that were unconnected with the parent martensite variant orientation, and therefore effectively randomized. In general, however, the present observation of concave post-irradiation curvature is consistent with a small amount of thermally-excited reversion of the previously deformed martensite in what amounts to an ion beam-induced shape-memory effect. Furthermore, for lower-dose, ambient temperature specimens F801–F803, there was a general tendency for this initial curvature to increase with the initial increase in temperature. This is consistent with an ion-induced reduction of the A_s temperature for any detwinned martensite that may have remained in the damaged zone.

The interpretation of the somewhat more pronounced concave curvature (curvature toward the irradiated face) at the edges of the irradiated zone is also complicated by uncertainties in the local specimen temperature. Here, it is simply noted that the effective irradiation temperature, if it were in fact elevated by beam heating above ambient, would have been lower at the margins of the irradiation zone due to the large in-plane stub loss there. It is further noted that pronounced concave curvature occurred only for the lower doses studied, and for the highest dose only at the irradiation zone margins (where a rapid dose falloff would occur). This is consistent with the idea that at higher doses ($> 5 \times 10^{13}$ cm^{-2}), beam damage may reduce the magnitude of reversion shape-strains by randomizing austenite nucleation as discussed above, or may induce sufficient disorder to fully inhibit any further displacive transformation activity.

Leaving aside now the post-irradiation concave curvatures, the most pronounced effect of irradiation in the present study was to cause a strong *convex* curvature (curvature away from the irradiated face) when the specimens were heated beyond the A_s temperature of the underlying, undamaged martensite phase. The most straightforward interpretation of this effect is that irradiation has

(even at low doses) effectively 'poisoned' the martensite-to-austenite transformation in the damaged zone, such that shape-recovery in the martensite (an axial contraction in the present case) stimulated a bending strain curving away from the irradiated face. This would certainly be expected to occur if the damage in the irradiated volume caused substantial amorphization, and would also be expected if sufficient disorder were induced to cause reversion in the damaged zone to occur with randomly-oriented nucleation of the austenite phase. In any case, the development of convex curvature was rapid and pronounced (often being limited by self-contact) and *thermally reversible*. Reversal of the curvature is consistent with the damaged layer responding in a nominally elastic way, so that during the reversion bending displacement strain energy was stored there and thus made available to re-deform the martensite phase on subsequent cooling. The observation that curvature reversal was not generally complete indicates that the initial martensite reversion strain produced a certain degree of irreversible plastic flow in the damaged layer. After the first few thermal cycles, however, a more-or-less stable 'two-way' shape-memory effect was exhibited by all of the irradiated specimens studied.

The force output measurements made here, though they were only approximate, indicate that ion-beam-induced two-way shape-memory is capable of delivering a non-trivial level of mechanical work. If the total active volume of the bending element is taken to be [4.28 mm $\times$ 6.53 mm $\times$ 6 μm] = 1.68×10^{-10} m^3, and the maximum force output is taken as 0.024 N at a tip-displacement of 1.5 mm, the approximate output energy density delivered by the element was on the order of 1.1×10^5 J/m^3. While this is only approx. 1% of the maximum practical energy density associated with SMA actuator materials [1], it indicates that, with optimization, the technique will be capable of producing forces that are highly competitive with other actuation schemes.

5. CONCLUSIONS

Based on these initial experiments on high-energy heavy-ion irradiation of pre-deformed titanium–nickel thin film martensite we conclude the following:

1. Irradiation to a dose of 5×10^{13} Ni^{2+} cm^{-2} produces a measurable increase in the elastic modulus and hardness of martensitic titanium–nickel thin films, and a dose of 1×10^{15} Ni^{2+} cm^{-2} results in approximately a twofold increase in maximum modulus in and threefold increase in hardness, as measured in nanoindentation experiments.
2. Irradiation to doses between 5×10^{13} and 5×10^{14} Ni^{2+} cm^{-2} lowers the canonical transformation temperatures in the titanium–nickel system but may not completely destroy displacive transformation capability.
3. Irradiation to a dose of 10^{15} Ni^{2+} cm^{-2} at 133 K does not in itself result in bending displacement of a deformed TiNi thin film martensite. However, lower doses delivered at temperatures closer to A_s can directly induce some bending strain.
4. Irradiation to doses greater than 5×10^{13} Ni^{2+} cm^{-2} frustrates shape-memory displacements normally associated with the reversion of a deformed martensite to the austenite. When beam damage is confined to a finite but limited depth in a thin film element, pronounced out-of-plane bending strains are generated.
5. At an irradiation dose of 10^{15} Ni^{2+} cm^{-2}, the beam-damaged zone may be plastically deformed by displacement of the underlying shape-memory layer, but is still capable of storing sufficient elastic strain energy to re-deform (or, 'reset') the shape-memory layer on subsequent cooling, leading to the realization of a two-way cyclic actuator element.
6. Such two-way actuator elements are capable of generating appreciable cyclic mechanical work output.

Acknowledgements—The authors wish to acknowledge Jinping Zhang at Michigan State University for his assistance in the fabrication of the thin films used in this study. We also give special thanks to Max Döbeli of the Paul Scherrer Institute for his assistance with ion irradiations at the Tandem Accelerator facility in Zurich, to Yves Bellouard and Hannes Bleuler of the Département de Micromechanique at EPFL for their help in making the force-output measurements, and to A. Karimi for his kind assistance with the nanoindentation study.

REFERENCES

1. Wolf, R. H. and Heuer, A. H., *J. Microelectromech. Syst.*, 1995, **4**, 1057.
2. Johnson, A. D., Busch, J. D. and Ray, C. A., *Mater. Res. Soc. Symp. Proc.*, 1992, **276**, 151.
3. Kuribayashi, K., Taniguchi, T., Ube, T., Yamaguchi, S., Yositake, M. and Ogawa, S., *Mater. Res. Soc. Symp. Proc.*, 1992, **276**.
4. Quandt, E., Halene, C., Holleck, H., Feit, K., Kohl, M. and Schlossmacher, P., in *Proc. 8th Int. Conf. on Sol. State Actuators: Eurosensors IX, Stockholm.* 1995, p. 282.
5. Hou, Li and Grummon, D. S., *Scripta metall.*, 1995, **33**, 989.
6. Grummon, D. S., Hou, Li and Pence, T. J., *J. Physi. IV*, 1985, **C8**, 655.
7. Hou, Li, Pence, T. J. and Grummon, D. S., *Mater. Res. Soc. Proc.*, 1995, **360**, 369.
8. Nomura, K. and Miyazaki, S., in *Proc. 1995 North American Conf. on Smart Structures and Materials*, 1995.
9. Hoshiya, T., Shimakawa, S., Ichihashi, Y., Nishakawa, N. and Wantanabe, K., *J. Nucl. Mater.*, 1991, **179**(181), 1119.

10. Hoshiya, T., Shimakawa, S., Ichihashi, Y. and Nishakawa, N., *J. Nucl. Mater*., 1992, **191**(194), 1070.
11. Hoshiya, T., Goto, I., Ohmi, M., Ando, H., Enami, K. and Nishakawa, N., *J. Nucl. Mater*., 1994, **212**(215), 1119.
12. Cheng, J. and Ardell, A., *Nucl. Instr. Methods*, 1990, **B44**, 336.
13. Goldberg, F. and Knystautas, E., in *SMST-97, Alisomar Conf. Ctr., Pacific Grove, CA*, 1997, p. 177.
14. Brimhall, J., Kissinger, H. and Pelton, A., *Radiat. Eff*., 1985, **90**, 241.
15. Zhang, J., Hou, Li and Grummon, D. S., *Proc. Mater. Res. Soc*., 1997, **459**, 451.